Self-consistent field theory of two-component phospholipid membranes

Nan Zheng,* J. Geehan,† and M. D. Whitmore
Department of Physics and Astronomy, University of Manitoba, Winnipeg, Manitoba, Canada R3T 2N2
(Received 21 October 2006; published 30 May 2007)

This paper extends and applies a self-consistent field theory of compressible, fully hydrated phospholipid bilayers to binary mixtures. The mixtures contain two kinds of lipids, which have identical head groups but different acyl chain lengths. The formalism we develop allows for the calculation of a range of thermodynamic and structural properties for systems at equilibrium, including the compatibility of the two components, the equilibrium phase, the bilayer thickness, the orientational order parameter profiles, and the ordering environment as a function of depth within the layer. Our focus in this paper is on the mutual effects of the different chains on each other, and the effects of the local environment on the order parameter of each segment in the chains, for systems in the fluid phase. We include an analysis of a feature of the order parameter profile identified as a "second plateau" by Morrow and co-workers [Biochemistry **32**, 290 (1993)].

DOI: 10.1103/PhysRevE.75.051922 PACS number(s): 87.14.Cc, 87.15.Aa, 87.16.Dg

I. INTRODUCTION

A major element of cell membranes belongs to a chemical class called phospholipids. These molecules are amphiphilic, and are usually composed of a hydrophilic phosphate headgroup and two hydrophobic hydrocarbon chains. When immersed in water, they can self-assemble into bilayers, with the headgroups in contact with the water and the chains forming the bilayer interiors. These bilayers can undergo a number of phase transitions; the main phases are the high-temperature, relatively disordered fluid phase, and the lower-temperature, relatively ordered gel phase. There are a number of other phases, including a relatively ordered, interdigitated gel phase. If the bilayers contain more than one kind of lipid, then the phase behavior can be much more complicated [1]. For example, the different lipids can separate into two different domains, either of which might be in the gel or fluid phase.

Lipid bilayers have been studied by a variety of techniques over the years. One useful tool is nuclear magnetic resonance (NMR). See, for example, Refs. [2–8]. NMR can give the orientational order parameter profile (OOPP) for lipids in the fluid phase, and can be used to identify phase transitions and boundaries in mixtures. We are interested, here, in the OOPP of lipids as measured by NMR experiments on lipids with fully deuterated chains. In these cases, each carbon has two deuterons bonded to it, except for the terminal one which has three deuterons. The orientational order parameter associated with a carbon unit n on a given chain is defined as

$$S_{\mathrm{CD}}(n) = \tfrac{1}{2}\langle 3\cos^2[\theta_{\mathrm{CD}}(n)] - 1\rangle, \qquad (1)$$

where $\theta_{\mathrm{CD}}(n)$ is the angle between the C-D bond and the reorientation axis, which is the bilayer normal. The angle brackets denote thermal averages taken over all the configurations of the chain, and the two, or three, C-D bonds at each carbon.

In this paper, we study fully hydrated bilayers which are compatible mixtures of two kinds of lipids, in the fluid phase. The particular lipids we consider are dimyristoyl phosphotidylcholine (DMPC) which has chains with length $l=14$, dipalmitoyl phosphotidylcholine (DPPC, $l=16$), distearoyl phosphotidylcholine (DSPC, $l=18$), diarachidonoyls phosphotidylcholine (DAPC, $l=20$), 1-stearoyl-2-oleoyl phosphotidylcholine (SOPC, $l=24$), and dipalmitoyl phosphotidylethanolamine (DPPE, $l=16$ as for DPPC, but a different headroup). In the mixtures we model, the lipids have identical headgroups but different chain lengths, e.g., DMPC with DPPC. The prime questions we address are twofold: What are the mutual effects of the long and short chains on each other's OOPP and can we relate these effects to the spatial distributions of the monomers?

Figures 1–3 show measured OOPPs for a number of systems and serve to clarify these questions. Two of these figures also show the values calculated using the theory of this paper. They will be discussed later; for now, we consider the measured values. In Fig. 1, the open circles represent the "smoothed" OOPP measured for DPPE at $T=69\ ^\circ\mathrm{C}$ [5]. "Smoothed" means that the values are arranged in monotonic, decreasing order. This profile has a plateau extending over about the first (upper) half of the chain, and then the $S_{\mathrm{CD}}(n)$ decrease in magnitude over the second (lower) half, to a final value on the order of $|S_{\mathrm{CD}}(16)| \simeq 0.05$.

It is worth noting that the relatively large drop in $|S_{\mathrm{CD}}(n)|$ at the terminal unit does not indicate a precipitous decrease in the order at the terminal unit. This can be understood by considering limiting cases. For all but the terminal unit, the values of $|S_{CD}(n)|$ can vary from 1/2 for a hypothetical, completely ordered chain section, to zero for a completely disordered section. This is because, in the fully ordered section, the two C-D bonds at each C lie in the plane perpendicular to the bilayer normal, and so $\cos[\theta_{\mathrm{CD}}(n)]=0$ and $|S_{\mathrm{CD}}(n)| = 1/2$. The situation is different for the terminal unit: Even in the fully ordered limit, the third C-D bond points out of this plane. The result is that the maximum value of $|S_{\mathrm{CD}}(n)|$, which is now an average over these three bonds, is signifi-

*Present address: Department of Physics, Duke University, Physics Bldg., Science Dr., Durham, NC 27708.
†Present address: University of Victoria, Victoria, BC, Canada.

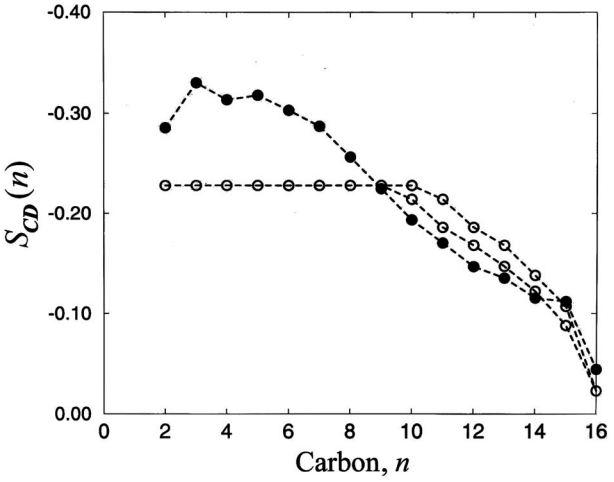

FIG. 1. Orientational order parameter profiles as functions of carbon number, $S_{CD}(n)$, for a typical one-component system, DPPE at $T=69$ °C. The two sets of open circles are the experimental values; they are the smoothed OOPPs for the sn-1 and sn-2 chains [5]. The filled circles are the OOPPs calculated with the theory used in this paper. This system, like all those of interest in this paper, is in the fluid phase. From Whitmore *et al.* [9]; reproduced with permission of National Research Council Press ©1998.

cantly reduced, by a factor of about 3. Decreases of this nature at the terminal unit occur for the disordered chains as well, and for all chains in all systems. They are simply due to the third bond pointing in a third direction.

Figure 2 shows the smoothed OOPPs in one- and two-component DMPC/DSPC systems [8]. The OOPP for pure DSPC is shown by the filled squares. These are the same in each panel, and are repeated for ease of comparison with the results for the mixtures. For this case, the $|S_{CD}(n)|$ decrease relatively slowly over about the first half of the chain, and then more rapidly over the second half. The profile for pure DMPC, filled circles, behaves in the same way, but is always somewhat smaller in magnitude than for the corresponding n in the long chain. Both profiles end at about $|S_{CD}(n)| \simeq 0.05$, the same as for DPPE. Although not as flat as in Fig. 1, the first part of these profiles is still often referred to as a plateau.

Now consider what happens to a system of short chains as longer chains are added in. This corresponds to moving from left to right on Fig. 2. Comparing the filled and open circles in panel (a), we see that addition of 25% longer chains induces more order among the short chains, i.e., the circles move up, although there is very little change for the terminal unit. The addition of more chains, e.g., 50% in panel (b) and 75% in panel (c), enhances this effect.

Complementing this picture, we can examine the effect of adding short chains to long chain systems. For this, we start with panel (c), and move left. Comparing the filled and open squares in panel (c), we see that the presence of 25% short chains reduces the order of the long chains. Moving across the panels to the left, we see that the addition of progressively more of the short chains further reduces the order of the long ones.

There is an additional effect not yet mentioned. In single component systems, the profiles always curve downwards for the outer parts of the chains, i.e., the slope becomes more negative with increasing n. This remains true for the short chains in the mixtures; in fact, adding long chains increases the magnitude of this curvature for the short chains. However, something different happens to the long chains. When there is a relatively low concentration of long chains in a short-chain host, e.g., the open squares in panel (c) of Fig. 2, then the profile for the units near the free end diverges from its normal shape: The curvature changes sign and is upwards, i.e., the slope becomes less negative. This feature was called a "second plateau" by Morrow and co-workers [2]. This feature does not include the terminal methyl unit itself, because of the third C-D bond as discussed above.

A third set of experimental results is shown in Fig. 3 [2]. These are for mixtures of 10 mol % concentrations of N-stearol galactosyl ceramide (18:0 GC) and N-lignoceroyl galactosyl ceramide (24:0 GC) in SOPC, at 52 °C. The host

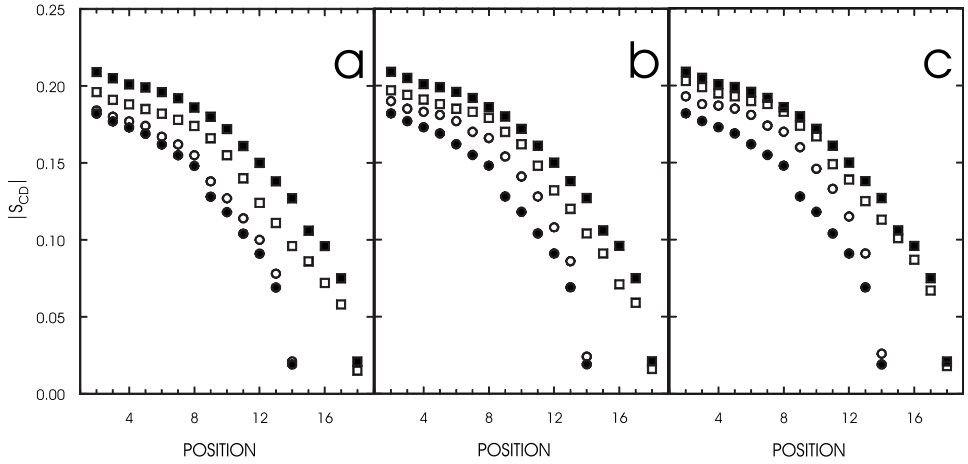

FIG. 2. Measured values of the smoothed OOPPs for mixtures of DMPC and DSPC at 60 °C. In each panel, the circles and squares show the profiles for the short and long chains (DMPC and DSPC), respectively. The filled symbols show the profiles in single component systems; they do not change from panel to panel. The open symbols show the profiles in the mixtures, and are different in each panel. The three panels are for mixtures containing 25%, 50%, and 75% DSPC. From Lu *et al.* [8]; reproduced with permission of the Biophysical Society © 1995.

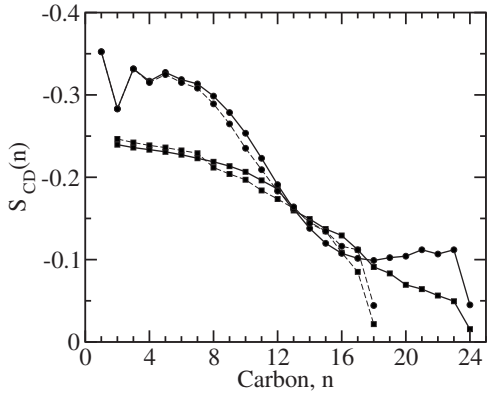

FIG. 3. Orientational order parameter profiles. There are two experimental systems: 10 mol % 24:0 GC in SOPC, and 10 mol % 18:0 GC in SOPC. Both are at 52 °C. The former is 5 mol % of longer chains. The calculations are for 5% of 24-unit chains in a host of 18-unit chains (DSPC) at 94 °C. The filled squares show the experimental results: Those joined by the dashed line are for the 18:0 GC, and those joined by the solid line are for the 24:0 GC. The filled circles show the theoretical values: Those joined by the dashed line are for the 18-unit chains, and those joined by the solid line are for the 24-unit chains.

SOPC molecules have two chains, each with 18 units, and each molecule has a double bond. The 24:0 GC also has two chains, one with 18 units and one with 24 units. Thus the mixture with 10 mol % of 24:0 GC molecules has only 5% long chains in a 95% short chain host. The 24-unit chain has no double bonds. The 18:0 GC also has two chains, but they both have 18 units. One of them has no double bonds. In both systems, the chains without double bonds were deuterated, and thus probed by the NMR. Thus one experiment probed 18-unit, saturated chains in a system where all chains are the same length, and the second experiment probed 5 mol % of 24-unit, saturated chains in a host of 18-unit chains. Comparing these measured profiles is analogous to comparing the profiles in a mix of 24- and 18-unit chains [2].

The results are shown in Fig. 3, and they are similar to those for the DMPC/DSPC blends. Over about the first 15 units, the $S_{CD}(n)$ for the short and long chains are nearly equal. For carbons $n \simeq 16$ to 18, the $|S_{CD}(n)|$ for the long chains diverge from those for the short chains. Beyond this n, units which of course only exist for the long chains, $|S_{CD}(n)|$ decreases, and finally ends at the same value as the terminal value for the short chains. The second plateau, noted above for DSPC in DMPC, is present again, and more prominent this time.

It is clear from these results that the long and short chains do influence the order parameter profiles of each other, but they are not rendered identical. Long chains enhance the order of short ones, and short chains reduce the order of the long ones. A second plateau appears for the long chains, and its prominence appears to be greatest at low long-chain concentrations, and for large differences in chain length.

In the rest of this paper, we examine these results and these systems by extending and applying a numerical self-consistent field (SCF) theory of lipid bilayers [9,10]. This theory is presented in Sec. II, with reference to Ref. [9] for many of the details that are common to the theory for single-lipid systems. Section III and the Appendices describe how we calculate the order parameter environment and spatial distributions as functions of position within the bilayer. Sections IV and V present our main results with detailed comparisons with experiments and an analysis of these results. Section VI summarizes our main conclusions.

II. THEORY OF TWO-COMPONENT LIPID BILAYERS

A. Fundamentals of the self-consistent field theory

The theory we develop here is an extension of the SCF theory we introduced in Refs. [9,10] for bilayers with one kind of lipid, which built on earlier self-consistent field theories of lipids [11–14]. It treats the gel, fluid, and interdigitated $L_\beta I$ phases within a unified framework, incorporates the effects of hydrostatic pressure, and permits the calculation of a range of structural and thermodynamic properties of the fluid phase and of the main transition.

The theory has a number of successes. It exhibits a first order, fluid ↔ gel phase transition (main transition), and indicates that the anisotropic bond dependence of the effective fields is essential to understanding this transition [15]. It predicts that the bilayer density changes by about 2%, and the bilayer thickness by about 30 to 35%, on going through the main transition [1,16]. Its predictions for the effects of pressure are of particular interest. First, it predicts that the main transition temperature increases with pressure, by about 17 °C per kbar for the specific case of DPPE. This compares with one measured value of about 18 °C per kbar for DPPE [20], and a range of values from about 15 to 23 °C per kbar for similar systems [17–32]. For bilayers in the fluid phase, the theory predicts that the isothermal application of pressure causes the layers to become *thicker* by about 2 to 3% per kbar [19,26,29], and the average order parameter to increase in magnitude by about 7 to 10% per kbar [32]. Finally, it predicts that, if both the temperature and pressure are increased in such a way as to move the system along the gel-fluid coexistence line, or at a fixed temperature interval above it, then the layer thickness and magnitude of the average order parameter *decrease*. This result, which represents a subtle competition between pressure and temperature, is, again, observed experimentally [32]. The theory gives reasonable agreement with the observed OOPPs, although with quantitative differences, and qualitative agreement with experiment for the chain length and head group dependences of properties of the main transition.

The new system is the same as in Ref. [9], except that there are two kinds of lipids. It consists of a mixture of lipid and solvent molecules at a temperature T and ambient pressure p_0, in equilibrium with a reservoir of excess solvent. Each lipid consists of a polar head group and two equal-length hydrocarbon chains. All headgroups are identical, but the two kinds of lipids have different chain lengths. In this paper, we assume the solvent is water.

We are interested in the periodic layered structure of the lipid-solvent mixture, at equilibrium. At any particular temperature and composition, the two kinds of lipids could mix or separate into two "macrophases," with one of them rich in

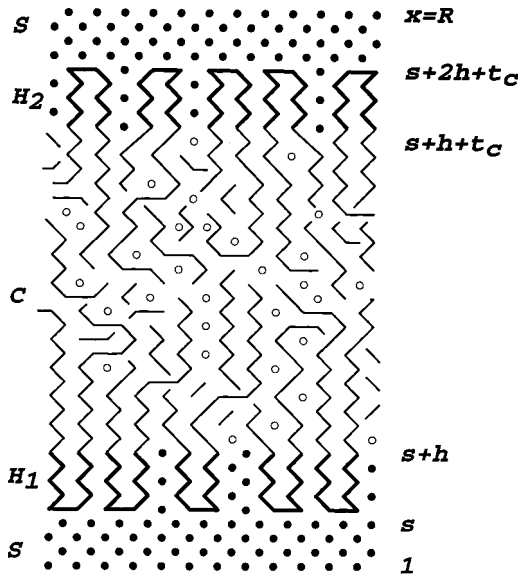

FIG. 4. Schematic representation of one unit cell of the model bilayer-solvent mixture. The head groups are represented by dark lines, the acyl chains by lighter lines, the solvent molecules by solid circles, and the vacancies by open circles. The broken lines within the C region represent chains projecting into and out of the plane, and so not all the hydrocarbon units are visible. The underlying tetrahedral lattice (diamond structure) is oriented so that the [110] direction, relative to the conventional cubic unit cell, is perpendicular to the plane of the bilayer. The bilayer consists of the t_C layers of region C which contains only hydrocarbon chains, plus the $2h$ layers of region $H=H_1 \cup H_2$ which contains the headgroups as well as solvent molecules. The bilayer is bordered on each side by region S which contains only solvent. The figure illustrates the case of $h=5$ and $l=16$, and interior and full bilayer thicknesses $t_C=22$ and $t_B=32$. All these correspond to DPPE very near to equilibrium in the L_α phase near the main transition. The density of vacancies is very close to zero in both the S and H regions, and there is no solvent in region C. For purposes of illustration, the free volume in the interior was chosen to be about twice as large as found in the calculations. From Whitmore *et al.* [9]; reproduced with permission of National Research Council Press © 1998.

long-chain lipids, and the other in short-chain lipids. Each phase could be fluid or gel. In this paper, we are interested in compatible, mixed lipids in the fluid phase. Fundamentally, our approach is to calculate the minimum free energy of the system under the assumption that the lipids in each layer are uniformly mixed, over the full range of composition. The existence of unstable mixtures, i.e., phase separation, is signalled by negative curvature in the function of the free energy vs composition.

The lipid-solvent mixture is a periodic, multilayer system. We envisage unit cells of area A and thickness R. Our model of one unit cell is illustrated schematically in Fig. 4. Each cell contains a number of sublayers, all with area A. One sublayer, or region, is the hydrocarbon interior of the bilayer, which we label C. There are two sublayers on either side of this, which we label H, that contain headgroups and solvent molecules. Finally, there is a region of pure solvent, S, between each bilayer.

Each solvent molecule is represented by a single structureless unit, which we label "s." For the lipids, we represent the headgroup and each chain by a series of these units. The headgroups are assumed to maintain a fixed size and shape, and are represented by two parallel series of units of fixed orientation perpendicular to the bilayer surface. The thickness of each headgroup layer is fixed at h layers. The internal conformations of each chain are described by sequences of trans and gauche isomers, and the thickness of the hydrocarbon interior, which we label t_C, is variable. The total thickness of each lipid bilayer is $t_B=t_C+2h$.

As discussed in Ref. [9], the model provides a reasonable representation of the size, shape and orientation of PE headgroups, but not the orientation of PC headgroups, which can change on passing through the gel-fluid transition. There can also be tilted chains in the gel phase. The model does not incorporate these effects. However, in this paper, we are considering only the fluid phase, and so these approximations are not a concern.

The starting point for the formalism is an expression for the partition function. We suppose the lipid-solvent mixture occupies a fixed volume V, and it contains fixed numbers of short and long lipids, N_l^1 and N_l^2. (We label the lipids with the shorter chains as "1," and those with longer chains as "2.") The number of solvent molecules present at equilibrium is controlled by the solvent chemical potential μ_s. With this notation, we introduce a mixed partition function,

$$\mathcal{Z}(T,N_l^1,N_l^2,\mu_s,V) = \sum_\Lambda \frac{(z_l^1)^{N_l^1}}{N_l^1!}\frac{(z_l^2)^{N_l^2}}{N_l^2!}\frac{z_s^{N_s^\Lambda}}{N_s^\Lambda!} \times \exp\{-\beta[(U^\Lambda + W^\Lambda) - \mu_s N_s^\Lambda]\}. \quad (2)$$

In this expression, Λ labels a particular configuration of the entire mixture, N_s^Λ is the number of solvent molecules present in that configuration, z_l^1, z_l^2, and z_s are the factors due to the kinetic energy of a short lipid, a long lipid, or a solvent molecule, U^Λ and W^Λ represent, together, the potential energy of configuration Λ, and $\beta=1/(k_BT)$, where k_B is the Boltzmann constant. The sum is over all possible configurations. Physically, this partition function is related to the Helmholtz free energy of the system, $\mathcal{A}$, via

$$-\frac{1}{\beta}\ln \mathcal{Z} = \mathcal{A} - \mu_s\langle N_s\rangle. \quad (3)$$

Equations (2) and (3) are the same as for the single lipid-solvent system, except for the presence of the factors due to the second kind of lipid in Eq. (2).

The first contribution to the potential energy, U^Λ, is the energy of the sequences of C-C bonds in all the lipid molecules. The second contribution arises from all the other interactions which, for convenience, are separated into hard core repulsions plus longer range parts. Because of the hard cores, no two atoms can occupy the same region of space, irrespective of whether they belong to the same molecule or two different ones. In principle, this is incorporated by including only those configurations Λ which satisfy this constraint. The energy due to the longer range part of the inter-

actions, which is denoted W^{Λ}, is a functional of the density distribution of each component in configuration Λ. We calculate it using two-body interactions.

As in Ref. [9], the partition function is converted to functional integrals over spatially inhomogeneous field variables, $\omega_k(\boldsymbol{r})$, that are introduced for each species, $\kappa=c$, h and s, i.e.,

$$\mathcal{Z}(T,N_l^1,N_l^2,\mu_s,V)=\frac{1}{\mathcal{N}}\prod_{\kappa,\boldsymbol{r}}\int_{-\infty}^{\infty}d\omega_\kappa(\boldsymbol{r})\exp(-\beta F[\{\omega_\kappa(\boldsymbol{r})\}]), \tag{4}$$

where $\mathcal{N}$ is a normalization and F is a free energy functional which can be written in terms of the fields, density distributions associated with each configuration Λ, and the interactions.

The integrations in Eq. (4) cannot be done exactly and are approximated by using the value of the integrand at its saddle point. Finding the saddle point yields a set of self-consistent equations for the equilibrium density distributions and fields $\omega_k(\boldsymbol{r})$. We set up our coordinate system so that the layers lie in the y-z plane and assume that the system is translationally invariant within these planes. We can then express the free energy for the layered system as

$$\beta F^0=-(I^0+\ln Q^0), \tag{5}$$

where

$$I^0=\frac{A}{2}\sum_{\kappa,x}\rho_\kappa^0(x)\omega_\kappa^0(x), \tag{6}$$

$$Q^0=\sum_{\Lambda}\exp\left\{-E_\Lambda^0+\sum_j[N_l^j\ln z_l^j-\ln N_l^j!\,]\right\}, \tag{7}$$

and

$$E_\Lambda^0=\beta U^\Lambda+\sum_{\kappa,x}N_\kappa^\Lambda(x)\omega_\kappa^0(x)-N_s^\Lambda(\ln z_s+\beta\mu_s)+\ln N_s^\Lambda! \tag{8}$$

In this expression, $N_\kappa^\Lambda(x)$ is the total number of units of type κ at x when the entire system is in state Λ, $\rho_\kappa^0(x)=\langle N_\kappa^\Lambda(x)\rangle/A$ is the average density of units of type κ at x, and the sums are over the entire multilayer system. The superscript "0" signifies that the corresponding quantity is calculated in the saddle point approximation.

We also reformulate the labeling of states by introducing states of individual molecules and associated occupation numbers. The state of a solvent molecule is specified simply by the plane on which it is located. The state of a lipid is specified by the plane of some part of it, and its internal state. We choose, without loss of generalization, the "labeling" part of the lipids to be the headgroup units that are bonded to the hydrocarbon chains. We model the internal states by embedding the molecules on a diamond lattice and using the rotational isomeric scheme (RIS) approximation to describe the C-C bonds on this lattice. The continuous variable x becomes a discrete one, labeling planes within the bilayers.

We label the state of a lipid by (x,λ,j), where x is the plane occupied by the labeling unit, λ specifies the bond sequence, and $j=1$ or 2 for a short or long lipid. The state of the entire system can be specified by sets of occupation numbers $\{N_\lambda^j(x)\}$ and $\{N_s(x)\}$, which denote the number of lipids of type j in each state (x,λ,j), and the number of solvent molecules on layer x, respectively. In general, a given set of occupation numbers corresponds to many distinct configurations, Λ.

Sums over states Λ are converted to sums over sets of occupation numbers via

$$\sum_{\Lambda}\cdots\rightarrow\sum_{\{N_\lambda^1(x)\},\{N_\lambda^2(x)\},\{N_s(x)\}}\frac{N_l^1!\,N_l^2!\,N_s!}{[\prod_{x,\lambda}N_\lambda^1(x)!\,][\prod_{x,\lambda}N_\lambda^2(x)!\,][\prod_{x,\lambda}N_s(x)!\,]}g\cdots. \tag{9}$$

The sums over lipid states are subject to the constraint that

$$\sum_{x,\lambda}N_\lambda^j(x)=N_l^j. \tag{10}$$

There is no corresponding constraint for the solvent; instead, N_s is simply the sum of the $N_s(x)$ for the configuration.

Equation (10) contains an important factor labeled "g." It incorporates the requirement that the sums over states exclude all those states for which sites would be doubly occupied. We calculate it in an approximate way that includes bond correlations [12,15]. On the diamond lattice, we need to specify two kinds of bonds for this purpose. Type 1 joins monomers in two adjacent planes, e.g., x and $x+1$, and type 2 joins two monomers that are in the same plane. The expression for g in Ref. [9] carries forward to the two component case:

$$g=\prod_x\frac{[A-\Psi_1(x)]\,![A-\Psi_2(x)]!}{A\,![A-N(x)]!}. \tag{11}$$

For a given configuration, $N(x)$ is the total number of units, c, h, and s, in plane x, $\Psi_1(x)$ is the number of bonds connecting units in planes x and $x+1$, and $\Psi_2(x)$ is the number of bonds within plane x. They include bonds within the headgroups as well as the acyl chains.

These latter quantities can be related to the occupation numbers by introducing two new sets of quantities. The first

set is $n^j_{c\lambda}(x'|x)$ and $n^j_{h\lambda}(x'|x)$, which are, respectively, the number of hydrocarbon and headgroup units on layer x belonging to one lipid of type j in state (x',λ,j). The second set is $m^j_{1\lambda}(x'|x)$ and $m^j_{2\lambda}(x'|x)$ which are, respectively, the number of bonds joining planes x and $x+1$, and the number of bonds lying within plane x, associated with a lipid of type j in state (x',λ,j). The relationships of quantities such as $N(x)$ and the $\Psi_b(x)$ to the occupation numbers are then given by straightforward generalizations of Eqs. (2.19) and (2.20) of Ref. [9], for example,

$$N(x) = \sum_{j=1}^{2} \sum_{x',\lambda} N^j_\lambda(x')[n^j_{h\lambda}(x'|x) + n^j_{c\lambda}(x'|x)] + N_s(x). \tag{12}$$

The summations over states still cannot be evaluated exactly, even after they are transformed according to Eq. (9), so a further approximation is made. Instead of summing over sets of occupation numbers, the summations are approximated by their summands evaluated using the most probable sets of occupation numbers. Maintaining the notation of Ref. [9], these sets, and the quantities calculated using them, are denoted by a "bar" over them. This represents the final major approximation, and results in the self-consistent field theory.

The system contains three distinct species, and so there are six pairs of two-body interactions, $c-c$, $c-h$, etc. We approximate them in the simplest possible way, as effective, nearest neighbor interactions. The expression for the self-consistent fields reduces to

$$\bar{\omega}_\kappa(x) = \beta \sum_{\kappa'} 4 W_{\kappa\kappa'} \langle \bar{\rho}_{\kappa'}(x) \rangle, \tag{13}$$

where each of the $W_{\kappa\kappa'}$ is characteristic of the overall strength of this part of the interaction, and $\langle \cdots \rangle$ denotes a local average, i.e.,

$$\langle \bar{\rho}_\kappa(x) \rangle = \tfrac{1}{4}[\bar{\rho}_\kappa(x-1) + 2\bar{\rho}_\kappa(x) + \bar{\rho}_\kappa(x+1)] \tag{14}$$

in the diamond lattice.

There are also occasions when a combination of interaction parameters that is very similar to the definition of Flory interaction parameters is useful, namely,

$$\chi_{\kappa\kappa'} = W_{\kappa\kappa'} - \tfrac{1}{2}[W_{\kappa\kappa} + W_{\kappa'\kappa'}]. \tag{15}$$

The values for the $W_{\kappa\kappa'}$ and $\chi_{\kappa\kappa'}$, along with a brief discussion of the implications of the nearest neighbor approximation for the potentials, are given in Ref. [9].

The density distributions need to be specified or calculated in each region. We assume the S regions are only solvent, so $\bar{\rho}_s(x) = \rho_0$ throughout, where ρ_0 is the normal solvent density. We assume that the acyl chains are confined to the interior C regions, so the H region contains only solvent and head headgroup units. In most expressions, we can also neglect the possibility of vacancies in this region. Hence, within H, we have a uniform headgroup density of $\bar{\rho}_h(x) = \rho_h$, and a uniform solvent density of $\bar{\rho}_s(x) = 1 - \rho_h$. This implies that the total density at any point in this region is unity, $\rho(x) = 1$, which we use except in expressions that involve $\ln[1-\rho(x)]$, which would diverge. In those cases, we use the corrections that are described in Ref. [9].

The heart of the calculation is the self-consistent calculation of the density within the C regions. Formally, there are two possible states for a headgroup complex in each unit cell, corresponding to either side of the bilayer. These states, which we label by $\sigma = \uparrow$ and $\sigma = \downarrow$, are mirror images of each other. It is straightforward to change the label of lipid states from (x,λ,j) to (i,σ,λ_c,j), where i denotes the unit cell containing the lipid, σ denotes the headgroup state we just defined, and λ_c denotes the state of the two hydrocarbon chains. We denote the mirror image of the state λ_c by λ_c^*; a lipid in state $(i,\uparrow,\lambda_c,j)$ is the mirror image of the lipid in state $(i,\downarrow,\lambda_c^*,j)$.

We assume that there are only c units in the C regions, but we also allow for vacancies. Now consider lipids in a particular unit cell, i. For lipids in each state (i,σ,λ_c,j), we define new quantities: $n^{j\sigma}_{\lambda_c}(x)$ is the number of hydrocarbon units on plane x and $m^{j\sigma}_{b\lambda_c}(x)$ is the number of bonds of type b, $b=1,2$, associated with plane x, belonging to a molecule of type j in configuration λ_c. We also define $n^{j\sigma}_h(x)$ and $m^{j\sigma}_{bh}(x)$, as the number of headgroup units and bonds at x associated with the headgroups.

The hydrocarbon and bond densities on plane x can be written in these terms as

$$\bar{\rho}_c(x) = \sum_j \frac{\rho^j_l}{\bar{Q}^j_c} \sum_{\lambda_c} [n^{j\uparrow}_{\lambda_c}(x) + n^{j\downarrow}_{\lambda_c^*}(x)] e^{-\epsilon^j_{\lambda_c}} \tag{16}$$

and

$$\bar{\psi}_b(x) = \sum_j \rho^j_l \Bigg[m^{j\uparrow}_{bh}(x) + m^{j\downarrow}_{bh}(x) + \frac{1}{\bar{Q}^j_c} \sum_{\lambda_c} \left[m^{j\uparrow}_{b\lambda_c}(x) + m^{j\downarrow}_{b\lambda_c^*}(x) \right] e^{-\epsilon^j_{\lambda_c}} \Bigg], \tag{17}$$

where

$$\bar{Q}^j_c = \sum_{\lambda_c} e^{-\epsilon^j_{\lambda_c}}. \tag{18}$$

In addition, for a lipid in state $(i,\uparrow,\lambda_c,j)$ (or its mirror image),

$$\epsilon^j_{\lambda_c} = \beta E_g \eta^j_\lambda + \sum_x n^{j\uparrow}_{\lambda_c}(x)[\bar{\omega}_c(x) - \ln(1-\bar{\rho}(x))] + \sum_{x,b} [m^{j\uparrow}_{b\lambda_c}(x) \ln(1-\bar{\psi}_b(x))]. \tag{19}$$

We also need

$$\bar{Q}^j_l = 2N_{\text{layers}} e^{-\epsilon^j_h} \bar{Q}^j_c, \tag{20}$$

where N_{layers} is the total number of bilayers in the system and

$$\epsilon^j_h = \sum_x n^{j\uparrow}_h(x)[\bar{\omega}_h(x) - \ln(1-\bar{\rho}(x))] + \sum_{x,b} [m^{j\uparrow}_{bh}(x) \ln(1-\bar{\psi}_b(x))]. \tag{21}$$

Equations (13)–(19) constitute the self-consistent problem to be solved for the $\bar{\rho}_c(x)$, $\bar{\psi}_b(x)$, and $\bar{\omega}_\kappa(x)$, for a system of lipids at a given thickness and density. They are very similar to the expressions in Ref. [9], with one important difference—the new index j. Equations (16) and (17) have summations over each kind of lipid. For each one, ρ_l^j is the average number density of lipid molecules of kind j at each interface. Thus these equations include contributions from lipids of each kind, and from each side. The exponential factors include the energy due to the gauche isomers in a molecule: E_g is the energy of a single gauche isomer, and $\eta_{j\lambda_c}$ is the number of gauche isomers in a molecule of type j in a state λ_c. The other terms in Eqs. (19) and (21) are interactions with the effective fields, that include effects of entropy and the bond correlations.

The form of these equations means that, in this mean field theory, each chain is moving in a field which is an average due to all the other chains. For a given field, we can treat short and long chains independently, but we then reconstruct the fields from the total densities due to all the chains. In the first step, we calculate each chain's properties by calculating and convolving two sets of propagators, labeled $G^{(n)}$ and $Q^{(n)}$. They are described in Ref. [9] and Appendix A of this paper. Each set is needed for $n=1,\ldots,l_2$. However, only a subset of each, for $n=1,\ldots,l_1$, is used for the short chains. The calculations of these propagators, and their convolutions for each kind of chain, are exactly as described in Ref. [9].

Once the SCF problem is solved, the minimized free energy for the layered system can be calculated from

$$\bar{F} = -\frac{A}{2\beta}\sum_{x,\kappa}\bar{\rho}_\kappa(x)\bar{\omega}_\kappa(x) - \sum_j \frac{N_l^j}{\beta}\ln\left(\frac{\bar{Q}_l^j z_l^j A}{N_l^j}\right) + \frac{A}{\beta}\sum_x [\ln(1-\bar{\rho}(x)) - \ln(1-\bar{\psi}_1(x)) - \ln(1-\bar{\psi}_2(x))]. \quad (22)$$

This is the same as for the single-component membranes, except for the summations over the two kinds of lipids in the second term. In evaluating the first term of this expression, we use $\bar{\rho}_S(x)$ as described above, and $\bar{\omega}_S(x)$ obtained from the density distributions via Eq. (13).

B. Equation of state and Gibbs free energy

Since the system incorporates the effects of pressure, we need to ensure both that the internal pressure is equal to the applied pressure, $p=p_0$, and that the free energy is minimized. The internal pressure can be calculated from our free energy via

$$p \to -\left(\frac{\partial F^0}{\partial V}\right)_{N_l^1,N_l^2,\mu_s} \quad (23)$$

i.e., holding lipid numbers, but solvent chemical potential, constant. Applying the procedure outlined in Ref. [9] to the new expressions for the mixtures leads to

$$\bar{p}t_B - 2hp_0 + 2s(\bar{p}-p_0) = W_{ss} + 2(W_{ch}-W_{cs})\rho_c^{(1)}\rho_h + (4-8h)\chi_{hs}\rho_h^2 + \frac{2}{\beta}[\ln(1-\rho_h/2)) - \ln(1-\rho_h) + \frac{1}{2}\sum_{x\in C} 4W_{cc}\bar{\rho}_c(x) \times\langle\bar{\rho}_c(x)\rangle - \frac{1}{\beta}\sum_{x\in C}[\ln(1-\bar{\rho}(x)) - \ln(1-\bar{\psi}_1(x)) - \ln(1-\bar{\psi}_2(x))], \quad (24)$$

where $\rho_c^{(1)}$ is the hydrocarbon density on the first layer of the hydrocarbon region, ρ_h is the headgroup density as discussed above, and χ_{hs}, which is defined by Eq. (15), represents an effective headgroup-solvent interaction. Equation (24) is the equation of state for the lipids.

We need the Gibbs free energy of the system. The mixture is in contact with the solvent reservoir, so the chemical potential of the solvent molecules must be independent of the structure of the lipids, and is therefore constant. Accordingly, we need consider only the partial Gibbs free energy of the lipids. Given that $F=A-\mu_s\langle N_s\rangle$, we have

$$\bar{G}_l = \bar{F} + \bar{p}V = \sum_j N_l^j\mu_l^j, \quad (25)$$

where μ_l^j is the chemical potential of a lipid of kind j. It can be written

$$\mu_l^j = \frac{1}{\beta}\ln\left(\frac{\bar{Q}_l^j A z_l^j}{N_l^j}\right). \quad (26)$$

Equations (24)–(26) are the same as for the single-component membranes, except for the summation in Eq. (25).

Since only variations in $\bar{G}_l$, rather than its absolute value, are important, we have the freedom to subtract off the Gibbs free energy of a reference state. The reference state we choose is the one in which all the lipids are fully extended and closely packed, in equilibrium with the bulk so that $\bar{p}=p_0$, and separated into two phases, with one phase composed of only short chains and having interior thickness $2l_1$, and the other having only long chains and interior thickness $2l_2$. The Gibbs free energy of this state can be obtained by considering each region separately, and recognizing that there are no gauche isomers, that all the bond densities are either zero or equal to the carbon or headgroup density on each layer, and that each $\bar{Q}_c^j$ depends only on interaction energies. Subtracting this from the Gibbs free energy yields our final expression for $\bar{G}_l$, which we write as the variation in free energy divided by the total number of lipids,

$$\frac{\Delta\bar{G}_l}{N_l} = 2h(p_0-\bar{p}) + (W_{hh}-W_{ss})\rho_c^{(1)} + 2(W_{ss}-W_{hs}) + 2\chi_{hs}[4h-1+(4-8h)\rho_h] + 2\chi_{ch}[\rho_c^{(1)}-1] - 2\chi_{cs}\rho_c^{(1)}$$

$$+\frac{1}{\beta}[\ln(1-\rho_h/2)+\ln(\rho_h/2)-2\ln(1-\rho_h)]$$
$$+\sum_j f_j\left[-2l_j\bar{p}-4l_jW_{cc}-\frac{1}{\beta}\ln\bar{Q}_c^j+\frac{1}{\beta}\ln f_j\right], \quad (27)$$

where χ_{ch} is defined by Eq. (15), and f_j is the number fraction of lipids of type j.

The two major results of this section are Eqs. (24) and (27) for the equation of state and partial Gibbs free energy, all of which are evaluated from the converged SCF solutions. The equilibrium repeat distance R, overall density and corresponding phase are determined by simultaneously requiring that $\bar{p}$ is the same as the ambient pressure, and by finding the value of R which minimizes the lipid partial Gibbs free energy, Eq. (27). Except for certain surface terms, the solvent between the bilayers contributes only to $\bar{p}$, and only through the term $2s(\bar{p}-p_0)$, which vanishes in equilibrium. This implies that the equilibrium state of our model membranes is independent of the thickness of the solvent region. Therefore, it suffices to minimize $\Delta\bar{G}_l$ with respect to the bilayer thickness, t_B or t_C, rather than R. Once we have obtained converged SCF calculations, we can identify the equilibrium thickness as the one with the minimum free energy, and complete the calculation of the properties of interest from the corresponding SCF solutions.

C. Stability of mixtures

Experimentally, all the systems we investigate in this paper form stable mixtures at the temperatures and compositions of interest. We can investigate the lipid compatibility within our approach by performing the full set of SCF calculations and calculating the free energy over the complete range of composition, i.e., we calculate $\Delta\bar{G}_l$ vs f_1 (or f_2) over $0\le f_1\le 1$. If there are compositions for which there would be phase separation, then there would be an interval of negative curvature in this function. Investigating the details of the phase separation would then involve locating spinodals and binodals. Uniformly positive curvature means that the lipids are compatible.

We have carried out these calculations for all the systems we discuss in this paper. The curvature was always positive for the cases we show here. Thus our calculations are in agreement with the basic observation that these systems are homogeneous mixtures in the fluid phase at these temperatures.

III. ORIENTATIONAL ORDER PARAMETER AND SEGMENT DISTRIBUTIONS

A. Orientational order parameter profile

The orientational order parameter was defined in the Introduction, Eq. (1). Here, we need to extend its definition to specify the kind of chain, j: Notationally, we replace $\theta_{CD}(n)$ and $S_{CD}(n)$ with $\theta_{CD}^j(n)$ and $S_{CD}^j(n)$. The order parameters are calculated from the propagators, as fully described in Ref. [9]. For example, for $2\le n\le l-2$,

$$S_{CD}^j(n)=\sum_x\sum_{x_0}\delta(x_0-(s+h+1))$$
$$\times\sum_{\beta_1\beta_2}\sum_{\beta_1'\beta_2'}G^{(n)}(x_0,x|\beta_2,\beta_1)P_{CD}^j(n,\beta_1,\beta_1')$$
$$\times\exp\{-[\epsilon_2(\beta_1,\beta_1')+\epsilon_3(\beta_2,\beta_1')+\epsilon_3(\beta_1,\beta_2')]\}$$
$$\times Q^{(l-n)}(x|\beta_2',\beta_1'). \quad (28)$$

In this expression, β_1 and β_1' are the bonds ending and starting at carbon n, β_2 and β_2' are the next bonds in each sequence, and

$$P_{CD}^j(n,\beta_1,\beta_1')=\tfrac{1}{2}\{3\cos^2[\theta_{CD}^j(n)]-1\}, \quad (29)$$

where $\cos^2[\theta_{CD}^j(n)]$ is the average for the two C-D bonds at n, which are defined by the bond sequence. The other two quantities are

$$e^{-\epsilon_2(\beta_1,\beta_1')}=\begin{cases}0, & \text{if } \beta_1 \text{ and } \beta_1' \text{ form backfolding,}\\ 1, & \text{otherwise}\end{cases} \quad (30)$$

and

$$\epsilon_3(\beta_1,\beta_2)=\begin{cases}0, & \text{if } \beta_1=\beta_2,\\ E_g/(k_BT), & \text{otherwise.}\end{cases} \quad (31)$$

The first of these eliminates bond sequences which correspond to backfolding and the second introduces the appropriate thermal factor if the sequence forms a gauche isomer.

B. Order parameter environment by layer

In experiments, the chains are constantly moving and changing shape and each carbon unit visits multiple layers during the effective averaging time of the measurement. Thus the usual definition of the order parameter describes one unit, n, which visits multiple layers. In this paper, we are also interested in the bilayer environment as a function of depth within the bilayer. We introduce the following two quantities, which describe the environment at a particular layer x as it is visited by different units from many chains.

(1) The average order parameter of all the units of a given chain as they visit a particular layer x. In contrast with the usual definition of the order parameter, this involves multiple units n and one layer x. To calculate it, we choose either a long or a short chain, tethered at one side, say $x_0=0$. We denote this quantity by $\langle S_{CD}^{(1)}(x)\rangle$.

(2) The average order parameter of all the units on layer x due to all the chains, long and short, starting from either side of the bilayer. We denote this by $\langle S_{CD}(x)\rangle$.

Both these quantities can be calculated from the converged SCF solutions, and the same propagators used for the usual order parameters. Details are given in Appendix A. The final expressions are very similar to the ones for the order parameter associated with a given carbon and they contain the same ingredients. However, for the order parameter associated with a given carbon, n is fixed and there are summations over x. For the order parameters associated with a given layer, x is fixed and there are summations over n.

C. Segment distributions

We will also probe where within the bilayer the free ends of the chains are found. Of course, they can be found on different layers, with different probabilities. In fact, this is true of any unit of any chain. Accordingly, we use the segment distributions of the carbons, $P_j(n,x)$, which we define as the probability that carbon n belonging to a chain of type j is on layer x. It depends on which type of chain the unit belongs to, and which side that chain starts from. These distributions can be calculated from the propagators: Details are given in Appendix B.

IV. RESULTS AND EXPERIMENTAL COMPARISONS

Figures 2 and 3 display the basic observations we are interested in understanding. First, pure long-chain systems are more ordered than pure short-chain systems. Second, when long chains are added to short-chain bilayers, the order of the short chains is enhanced, except for the terminal unit. Finally, when short chains are added to long-chain bilayers, the order of the long chains is reduced, except for the terminal unit, *and* a second plateau develops. The value of the order parameter for the terminal units of the long and short chains are nearly the same, about a third of the values for the penultimate units.

We begin the discussion of the theoretical results by returning to Fig. 1. The filled circles on this figure are the OOPPs for pure DPPE, calculated earlier with the SCF theory used here [9]. As in the experiments, the theoretical $S_{CD}(n)$ have an initial plateaulike region, and this is followed by a decrease. The overall average order parameter, i.e., the average over all n, is −0.21 in the theory, close to the experimental value of −0.19 [9].

In contrast with the experimental results shown in Figs. 1–3, the theoretical profiles are nonmonotonic in the plateau region. This difference is attributable to the fact that the experimental results are smoothed, with monotonicity imposed. Experimental profiles that are not smoothed show similar variations [3]. However, even after allowing for the nonmonotonicity, the theoretical plateau is still steeper than the measured one shown for DPPE. On the other hand, it is similar to the experimental profiles for the other cases, shown in Figs. 2 and 3. Two differences remain: The calculated values of $|S_{CD}(n)|$ in this first plateau are greater than the measured ones, and there is already a small second plateau near the free end of the chain. We shall return to both these points.

We turn now to our new results for mixtures. All the rest of the cases we treat in this paper are for phosphotidylcholine (PC) headgroups, which correspond to $h=6$ in our model. We use appropriate chain lengths as described below for each case. All other parameters are given in Ref. [9].

Figure 5 shows our calculated OOPPs for the short and long chains in DMPC/DPPC (upper panel), DMPC/DSPC (middle panel), and DMPC/DAPC (lower panel) mixtures, all at 65 °C. In these systems, the short chains are the DMPC, with $l_1=14$, and the longer chains are, respectively, $l_2=16$, 18, and 20. The middle panel is for the same system as in Fig. 2. Each panel shows the results for three compositions.

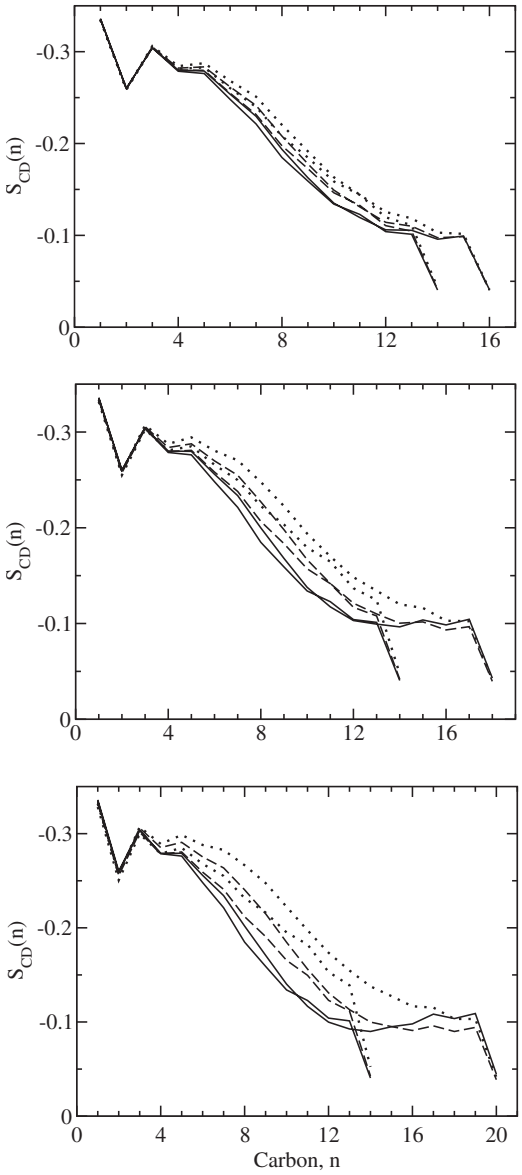

FIG. 5. Calculated OOPPs for mixtures of long and short chain lipids at 65 °C in three different sets of mixtures. The top panel is DMPC and DPPC ($l=14$ and 16), the middle panel is DMPC and DSPC ($l=14$ and 18), and the lower panel is DMPC and DAPC ($l=14$ and 20). In each panel, the short solid curve is for pure short chains (DMPC), the long solid curve is for one isolated long-chain molecule in a short-chain host, the dashed curves are for equimolar mixtures of long and short chains, the long dotted curve is for pure long chains, and the short dotted curve is for an isolated short-chain molecule in a long-chain host.

We begin with the upper panel. It is for DMPC and DPPC, which have a chain length difference of two units. The short, solid curve is pure DMPC, and the longer dotted curve is pure DPPC. The curves are qualitatively similar to each other, and to those in Figs. 1–3. They start at a common value, $|S_{CD}(1)| \simeq 0.33$, initially oscillate, and then decrease monotonically to a common final value of about 0.04. Throughout most of the chains, from $n \simeq 3$ to $n \simeq 13$, each

$|S_{CD}(n)|$ for the longer chain is greater than for the corresponding unit of the shorter chain and the overall average is greater for the longer chain.

The other curves show the effects of mixing. The long dashed curve shows the effect of adding 50% short chains to the long chains: The order parameter of each unit of the long chain is reduced, except near each end of the chain. The long solid curve shows the limiting case of enough added short chains that only isolated long chains remain: The order is reduced even further, except near the free end. The remaining curves show the effects of mixing on the short chains: Adding long chains increases the order of each unit of the short chains, except for the units near the headgroup, and the terminal unit at the other end. Notice that, when one long chain is immersed in a sea of short chains, the order parameters for the n units of the long chain up to unit l_1-1 are very similar to those of the short chain. Similarly, for one short chain in a sea of long chains, the $S_{CD}(n)$ on the short chain are comparable to those of the long chain. All this is in qualitative agreement with the experimental results shown in Figs. 2 and 3. The second plateau is also apparent here. In fact, it is much more pronounced in the theoretical results than in the experimental ones.

The remaining panels of this figure show the effects of increasing differences in chain lengths, to 4 and 6, respectively. There are both quantitative and qualitative effects. First, $|S_{CD}(n)|$ for each unit on a long chain in pure long chains is always greater than that of the corresponding unit on a short chain in a system of pure short chains, except very near each end. The differences increase with increasing chain length difference. Second, for one long chain in a short-chain host, each $|S_{CD}(n)|$ is reduced to about the same value as that of the corresponding unit of the host short chains for n up to l_1-1. Third, for an isolated short chain in a long-chain host, the $|S_{CD}(n)|$ is increased, but not all the way to the values for the long chains. Finally, the long chain profiles always exhibit a second plateau, which is very pronounced when the chain length difference is large and the proportion of long chains is low.

Figure 3 includes a direct comparison of our theoretical results with the experiments on the GC/SOPC systems. As argued in the Introduction, the experiments correspond to 5 mol % of 24-unit chains and a host of 18-unit chains, and so we chose this composition for these calculations. We also had to choose a suitable temperature. The double bonds of the SOPC molecules in the experiments lower the main transition temperature and influence the environment, but there are no double bonds in the host DSPC of the calculations. Therefore, we used a temperature which is the same relative to the main transition in each case. For SOPC, this transition temperature is 6 °C, and the experiments were done at 52 °C, which is 46 °C higher. The transition temperature of DSPC is about 48 °C, so we used $T=94$ °C.

The experimental results were described in Sec. I. Comparing our theoretical results and the experimental ones yields three main observations. First, in both the theory and experiment, the OOPPs for the short and long chains are nearly equal over most of the length of the short chains; this extends up to $n \simeq l_1-1$ for the theoretical results. Second, the order parameter values for the terminal units of the long and short chains are about equal. Third, both theoretical and experimental values show pronounced second plateaus for the longer chains, for $n \gtrsim l_1$. Finally, this second plateau is much more pronounced in the theoretical results than in the experiments.

We draw the following conclusions from this. First, the order parameter of a unit depends on which chain it is on, where it is on that chain, and the presence of other chains, i.e., the long and short chains do influence each other. Next, a second plateau develops for the long chain, and it is greatest for large chain-length differences and low long-chain concentrations. Third, as in the single-lipid systems, the $|S_{CD}(n)|$ for units in the first half of the chain are larger in the theory than experimentally. Finally, the second plateau in the theoretical results is much more pronounced than in the experiments.

V. INTERPRETATION: ORDER PARAMETER ENVIRONMENT

We now want to probe in more detail the reason for the changes in the OOPPs and the mutual effects of the long and short chains. We will argue that the second plateau is due to the penetration of the longer chains beyond the middle of the bilayer and suggest why the theory produces a too-prominent second plateau. We will examine the thickness of bilayers in the mixtures, where the free ends of the long chains are within the bilayers, and the ordering environment in the region where these ends tend to be.

We begin by examining the equilibrium thicknesses of the mixtures, and the spatial distributions of the terminal unit of each chain. Figure 6 shows the thickness as a function of composition, for three sets of blends. The left-hand side of the figure corresponds to pure DMPC, with a thickness of about 19 units. The right-hand side is pure DPPC, DSPC, or DAPC, with layer thicknesses of about 21.5, 24, and 26 units, respectively. (The thickness is in units of 1.25 Å, which is the length defined by the projection of a C-C bond along the bilayer normal.) For blends, the thickness increases smoothly, and nearly linearly, with long-chain concentration.

Figure 7 shows the spatial distributions of the terminal units, $P_j(l_j,x)$, for each chain for these systems at three concentrations. They all have the same general shape, starting at values of $P_j(l_j,1) \simeq 0.03$, rising to a maximum, and then decreasing to zero. A chain of l_j units can only reach to layer $x=l_j$, and then only when it is fully extended, so each curve falls to zero beyond that layer.

Consider the short chains first. For pure DMPC, $P_1(l_1,x)$ is shown as the shorter solid curve, terminating at $x=14$ for these 14-unit chains. This curve is the same in all three panels. Its maximum is just before $x \simeq 10$. We can see from the left-hand intercept of Fig. 6 that this system has a thickness of about 19 units, so the peak in this distribution is very close to the bilayer center. As longer chains are added, the peak moves slightly to larger x, and the bilayer gets thicker. For example, for a 50:50 mixture of DMPC and DPPC, the shorter dashed curve in the upper panel, the peak is closer to $x \simeq 10$, but the layer thickness has increased to $t_C \simeq 20$, so the

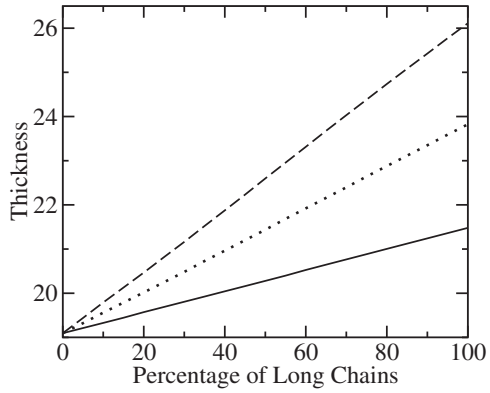

FIG. 6. Calculated thickness of the hydrocarbon interior of the bilayer for DMPC/DPPC (solid curve), DMPC/DSPC (dotted curve), and DMPC/DAPC (dashed curve) mixtures, as functions of the percentage of long-chain lipids, at 65 °C. Each thickness is calculated through the full SCF calculation and minimization of the free energy. The left-hand side represents pure DMPC, and the right-hand side pure DPPC, DSPC, and DAPC. The thickness is in units of 1.25 Å, which is the length defined by the projection of a C-C bond along the bilayer normal.

peak is still very near the center. For a single DMPC in DPPC, the shorter dotted curve, the peak is just beyond $x \simeq 10$ and the thickness has increased to $t_C \simeq 21.5$. In all these cases, the peak in this distribution for the short chain ends is very close to the center of the bilayer. In blends of greater difference in chain length, the peak in $P_1(l_1,x)$ can be before the bilayer center. For example, in the limiting case of a single 14-unit chain in a 20-unit host, the shorter dotted curve in the lowest panel, the peak is at $x \simeq 11$, the layer thickness is $t_C \simeq 26$, so the bilayer center is at about $x \simeq 13$. We conclude that the peak in the spatial distribution of the short chains' ends is always at or before the bilayer center.

Now consider the long chains. Pure long-chain systems behave the same way as the pure short chain systems. These are the longer dotted curves in each panel of Fig. 7. Their maxima are at about $x \simeq 11, 12$, and 13 for $l_2 = 16$, 18, and 20, respectively. As noted above, the corresponding layer thicknesses are $t_C \simeq 21.5$, 24, and 26, so the maxima in $P_2(l_2,x)$ are very close to the bilayer centers. As short chains are added, the layers get thinner and the peak in $P_2(l_2,x)$ moves to the left. Now we get a slightly different result: Comparing the distribution functions for the long chains with the layer thicknesses, we find that the peak is always very close to the bilayer center. We thus conclude that the peak in $P_2(l_2,x)$ for the long chains is always very close to the bilayer center and the peak in $P_1(l_1,x)$ for the short chains is always very close to, or before, the bilayer center.

The location of these maxima is only one feature of these distributions: Their shape beyond the peak is also important. For the short chains, $P_1(l_1,x)$ always decreases from its maximum to zero over a short distance and there is very little penetration of the short chains beyond the bilayer center. This is also the case for pure long chain systems, but *not* for long chains in short-chain hosts: $P_2(l_2,x)$ always extends to $x \simeq l_2$, even when the bilayer is almost entirely composed of short chains. In such cases, the peak in $P_2(l_2,x)$ can be at

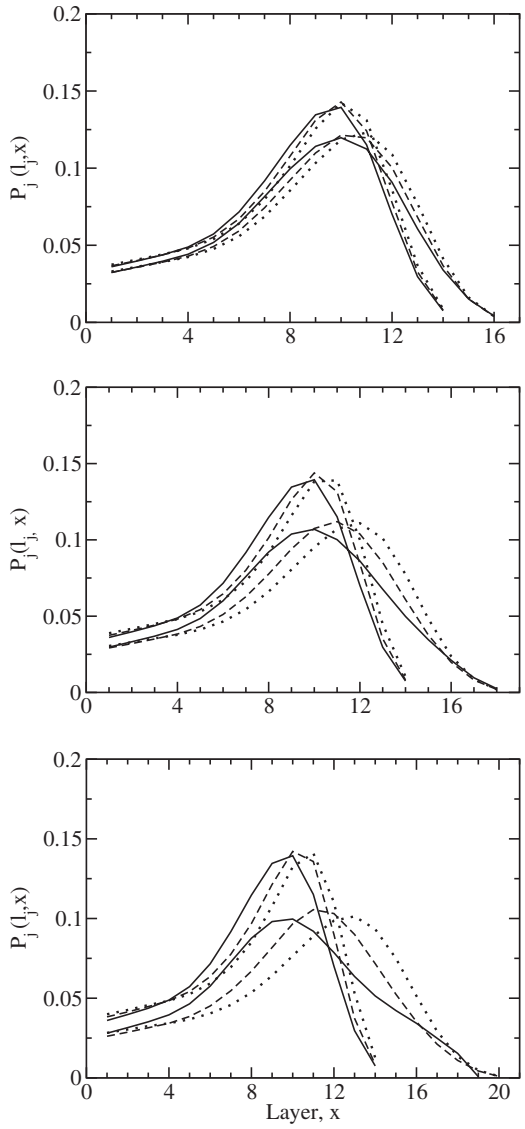

FIG. 7. Spatial distribution functions for the end segments of long and short chain lipids at 65 °C in three sets of mixtures. The panels and notation are the same as in Fig. 5. The top panel is DMPC/DPPC, the middle panel is DMPC/DSPC, and the lower panel is DMPC/DAPC. In each panel, the solid curves are for the case of pure short chains or one isolated long-chain molecule in a short-chain host, the dashed curves are for equimolar mixtures of long and short chains, and the dotted curves are for the case of pure long chains or an isolated short-chain molecule in a long-chain host. The unit of length is 1.25 Å.

$x \simeq 10$ to 12, but there is a long tail extending well into the second half of the bilayer. This tail can be quite long, as seen in particular in the lowest panel of Fig. 7. In fact, for the case of the 14/20 bilayer at very low long-chain concentrations, the tail would penetrate entirely through and past the carbon region, if this were not prevented by the strong repulsion of the distant head groups. Overall, we conclude that the short chains do not penetrate very much beyond the bilayer center, but the long chains can, especially for a large chain length difference and low long-chain concentrations.

We next examine the local ordering environment that the carbons experience and for this we use $\langle S_{CD}(x) \rangle$, the average

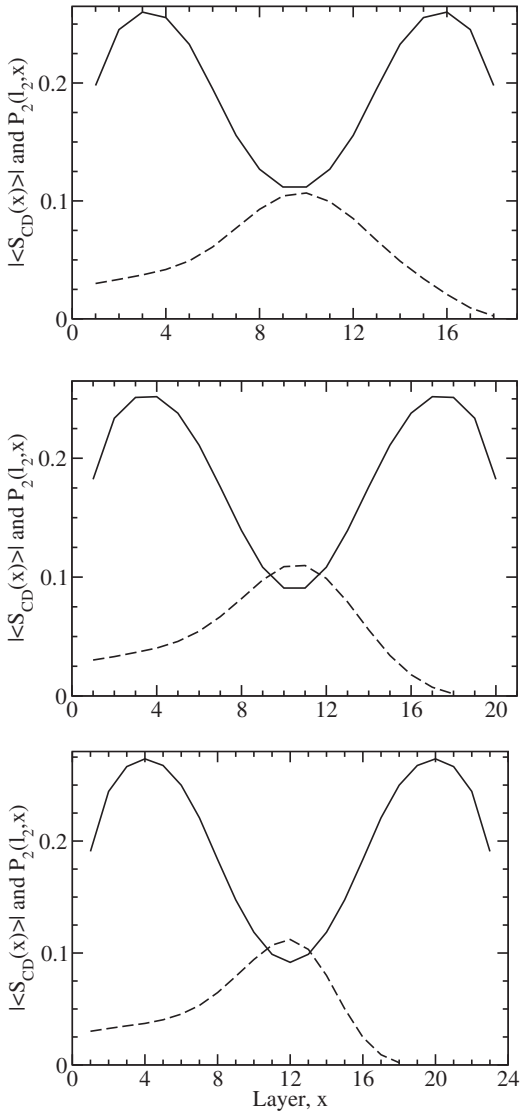

FIG. 8. Average orientational order parameter on each layer, and the spatial distribution function of the end segment of DSPC, in DMCP/DSPC systems at 65 °C. The upper panel is for the case of one isolated DSPC molecule in DMPC, the middle panel is for an equimolar mixture, and the lower panel is for pure DSPC. In each panel, the upper curve is the average orientational order parameter by layer and the dashed curve is the spatial distribution function of the end segment of DSPC.

order parameter on each layer. This is shown in Fig. 8 for one of the sets of mixtures just discussed, DMPC/DSPC, that was illustrated in the middle panel of Fig. 7. The upper panel of Fig. 8 is for a system with one DSPC molecule in a DMPC host, the middle panel is for a 50:50 mixture, and the lowest panel is for pure DSPC. There is an inherent ambiguity in the interpolations of $\langle S_{\mathrm{CD}}(x)\rangle$ to nonintegral layer thicknesses, so these are shown for the integer thickness closest to the equilibrium thickness in each case.

In all cases, $|\langle S_{\mathrm{CD}}(x)\rangle|$ starts at a value of about 0.2, rises to a maximum value of about 0.25 approximately 1/6 of the distance into the bilayer, and then decreases to a minimum value of about 0.1 at the center. It is, of course, symmetric about the bilayer center. The initial values of $|\langle S_{\mathrm{CD}}(x)\rangle|$, i.e., nearest the headgroup, are similar to those of $|S_{\mathrm{CD}}(n)|$ for the carbon units in the first half of the chain, the subsequent decrease with x resembles the decrease in $|S_{\mathrm{CD}}(n)|$ for units in the second half of the chain, and the minimum at the center is similar in value to the $|S_{\mathrm{CD}}(n)|$ for the units near the free end.

To bring the discussion of the origin of the plateau to a conclusion, we now turn to the environment sampled by the hydrocarbons near the free ends of the long chains, and how it changes in the mixtures. Figure 8 also shows the spatial distribution functions for the terminal unit of the long chains for the corresponding integer thickness. In all cases, as noted above, the maximum in $P_2(l_2,x)$ is always at the center of the bilayer, which is the most disordered region with the minimum in $|\langle S_{\mathrm{CD}}(x)\rangle|$, and the tail of the distribution always extends out to layer 18. However, further details are revealing. In the pure long-chain system, lower panel, the layer thickness is about 24, and the end-segment distribution ends at layer 18. By comparing the two curves in this panel, we see that, although the chain can penetrate beyond the center with nonzero probability, it does not reach beyond layers in which the environment is relatively disordered, i.e., beyond layers where $|\langle S_{\mathrm{CD}}(x)\rangle|$ is small. In the 50:50 mixture, middle panel, the thickness is reduced to about 21, but $P_2(l_2,x)$ still reaches to layer 18. This means that the long chains can reach to within two or three layers of the distant side. Comparing the two curves in this panel, we see that, this time, the long chains can penetrate into the region where $|\langle S_{\mathrm{CD}}(x)\rangle|$ increases with proximity to the distant surface. For the limiting case of one long chain in an otherwise pure short-chain system, upper panel, the thickness is reduced to just $t_C \simeq 19$, $P_2(l_2,x)$ still reaches to layer 18, and the free ends of the chains have a significant probability of penetrating well into the region of relatively high order, in the distant half of the bilayer. When this occurs, units near, but not at, the free end of the chain are close to the most disordered bilayer center.

Overall, we have a picture of the long chains being able to penetrate past the bilayer center into the distal half of the bilayer where the environment is more ordered, and this effect increasing as the concentration of long chains decreases. This correlates well with the second plateau that occurs for the long chains but not the short ones, and that is most prominent when the concentration of long chains is lowest. Units adjacent to the free end of the chain have enhanced order, and the units just prior to them are close to the bilayer center so have reduced order. Although this discussion has focussed on only 18/14 blends, the same effects occur for other chain length differences.

To probe further into the details, we consider $\langle S_{\mathrm{CD}}^{(1)}(x)\rangle$ for these same systems. Our results are shown in Figs. 9 and 10. As described in Sec. III B, this is the average order parameter of all the units on chains attached to the left side which are on layer x.

Any unit n can reach, at maximum, only to layer $x=n$. Conversely, on each layer x, $\langle S_{\mathrm{CD}}^{(1)}(x)\rangle$ has contributions only from units $n=x$ to l_j. For example, only the terminal unit, $n=l_j$, can reach layer $x=l_j$, so only that unit contributes for that layer. The last two units, $n=l_j$ and l_j-1, can reach layer $x=l_j-1$, and contribute to that $\langle S_{\mathrm{CD}}^{(1)}(x)\rangle$, and so on. This im-

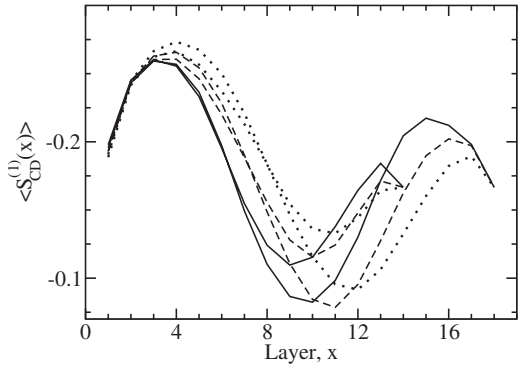

FIG. 9. Average orientational order parameter on each layer for chains attached to the left side, $\langle S_{CD}^{(1)}(x)\rangle$, for long and short chains in binary bilayers of DMPC and DSPC at 65 °C. The notation is the same as in Fig. 7: The solid curves are for the case of one isolated DSPC molecule in a DMPC host, the dashed curves are for equimolar mixtures, and the dotted curves are for the case of one isolated DMPC molecule in a DSPC host. The short curves are for the DMPC and the longer ones for DSPC.

plies that the layers most distant from the tethering point have contributions mainly from units near the chain's free end. On average, these units are relatively disordered, and so one might expect that $|\langle S_{\mathrm{CD}}^{(1)}(x)\rangle|$ would decrease monotonically with x, in a fashion qualitatively similar to the way $|\langle S_{\mathrm{CD}}(n)\rangle|$ normally decreases with n.

This is not the case. All the curves start at about the same value, rise to a maximum, decrease to a minimum, rise again to a secondary maximum, and then, except for one case, decrease again. They all terminate at the layer corresponding to the chain length, and they all terminate at the same value.

The behavior for the initial layers is straightforward to understand. For layers close to the left side, only chains originating there can contribute; those from the other side cannot reach, or do so with only very low probability. Thus the $\langle S_{\mathrm{CD}}^{(1)}(x)\rangle$ for each chain follows the overall $\langle S_{\mathrm{CD}}(x)\rangle$ in this region. The fact that all the curves terminate at the same value can be understood from a slightly different perspective.

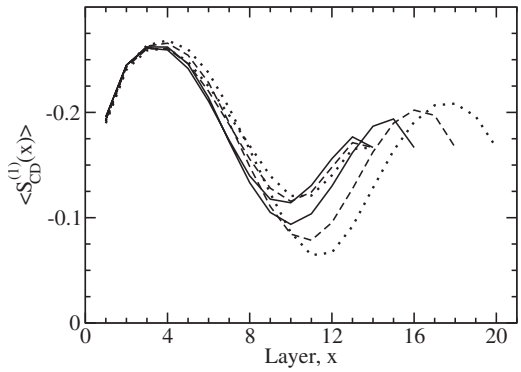

FIG. 10. Average orientational order parameter on each layer for chains attached to the left side, $\langle S_{CD}^{(1)}(x)\rangle$, for long and short chains in equimolar binary bilayers for three different systems at 65 °C: DMPC/DPPC (solid curves), DMPC/DSPC (dashed curves), and DMPC/DAPC (dotted curves). The short curves are for the DMPC and the longer ones for DAPC.

This common value is due to the terminal unit *when it is on the farthest layer it can reach.* It does this only when the entire chain is fully ordered. This is a rare event, but it is the only one that contributes to this particular $\langle S_{\mathrm{CD}}^{(1)}(x)\rangle$. The value in this case is $\langle S_{\mathrm{CD}}^{(1)}(x)\rangle = -1/6$.

To analyze the other curves, it is useful to consider the concentration dependences at the same time. Consider first the long chains. For pure DSPC, Fig. 9, the order is relatively high in the first half of the bilayer, decreases to a minimum, then increases again for layers beyond the center, where the chain ends are penetrating into the more ordered parts of the chains tethered to the other side. As short chains are added in, the bilayer gets thinner, and the relatively ordered first half of the chain becomes less ordered, so $|\langle S_{\mathrm{CD}}^{(1)}(x)\rangle|$ decreases. However, on layers beyond the bilayer center, $|\langle S_{\mathrm{CD}}^{(1)}(x)\rangle|$ increases. This occurs as the penetration of the long chains beyond the center increases, as discussed above. For the short chains, adding long chains increases the order almost everywhere: the exception is very near the free end, where there is a slight reduction. It is reasonable to attribute this last feature to the reduced penetration of the short chains beyond the center in the mixture, but this penetration is always small, so the resulting effect is also small.

We end this section with Fig. 10, which shows $\langle S_{\mathrm{CD}}^{(1)}(x)\rangle$ for 50:50 mixtures, but different systems. The messages of this figure are that those systems behave in the ways just examined, but the difference between the minimum and the second maximum increases significantly with increasing difference in chain length. This difference correlates with the strong dependence of the prominence of the second plateau on the chain length difference.

VI. DISCUSSION

In this paper, we have extended an SCF theory of bilayers to the case of compatible mixtures of lipids which have the same headgroups but different length acyl chains, and are in the fluid phase. The primary experimental results we have probed can be summarized as follows. First, the long and short chains influence the order parameter profiles of each other, with the long chains enhancing the order of the short ones and the short chains reducing the order of the long ones. Second, when the concentration of long chains is very low, the order parameter profiles over the first parts of the two chains are nearly equal. Finally, a second plateau appears for the long chains, and it is most prominent at low long-chain concentrations, and for large differences in chain length. It does not include the terminal unit.

The theory is in qualitative agreement with these results, and we used it to explore, in particular, the second plateau. We concluded that the order parameter of a carbon unit depends on which chain it is on, where it is on that chain, and where it is within the bilayer. By examining the equilibrium layer thickness, the spatial distributions of the terminal units of each chain, and the ordering environment as a function of position within the bilayer, we obtained a consistent picture of the second plateau. The peak in the distribution function for the end unit of the long chains is always very near the

bilayer center. However, when the long chains are a minority component, this distribution has a long tail, and these chains can penetrate past the disordered center of the bilayer, reaching into the far side where the average order increases again. This penetration is greatest for the last unit at the long chains' free ends, so units adjacent to it become more ordered. In this case, units near, but not at, the free end are pulled to the vicinity of the disordered bilayer center, and have diminished order. The result is the second plateau. The penetration increases with increasing difference between the lengths of the long and short chains. It also increases as the concentrations of long chains decreases, primarily because the bilayer becomes thinner in that case.

There are two related features of the theoretical profiles that warrant future attention. One is that, even for single component lipids, the magnitude of the $S_{\mathrm{CD}}(n)$ for the first half of the chain is greater than observed experimentally, i.e., the first plateau is too high. The other one is that the second plateau is too prominent. This second feature may be a consequence of the first. We argued that the second plateau is due to the penetration of the free ends of the long chains into the more ordered region in the distal half of the bilayer: The greater order there induces more ordering of the units penetrating into it. However, this is the region which is occupied largely by the first half of the apposing chains, i.e., the units that form the first plateau. Since the theory predicts too much order for these units, it would not be surprising if it predicts too much order for the units penetrating into them. Stated another way, within the theoretical results, the overly enhanced ordering of the upper half of the chains attached to one side of the bilayer overly enhances the second plateau of the chains attached to the other side. It is also possible that the theory predicts too much penetration of the long chain past the bilayer center. These factors would also explain the presence of the incipient second plateau in the single-component systems.

Why the theory predicts more order in the first plateau than is observed is an unanswered question, especially in view of how well it predicts numerous other properties. We end by speculating that likely reasons are the assumption of a very narrow headgroup-hydrocarbon interface, coupled to the use of the RISM approximation and diamond lattice to describe the conformations of the chains. These approximations are constraints on the configurations of the parts of the chains near the headgroups, constraints which could enhance the predicted degree of order for these units. The exploration of these approximations awaits further work.

ACKNOWLEDGMENTS

We thank Dr. M. R. Morrow and Dr. J. P. Whitehead for many helpful discussions. We particularly thank Dr. Morrow for his experimental data and help with Fig. 2. The work is funded by the Natural Sciences and Engineering Research Council of Canada, and the Canada Foundation for Innovation.

APPENDIX A: CALCULATION OF THE ORDER PARAMETER ENVIRONMENT BY LAYER

In this appendix, we outline the derivation of the calculation of two quantities describing the order parameter environment by layer that were introduced in Sec. III B.

Our final expressions all use the same sets of propagators that are used in the SCF calculation. One set, those of type G, describe chain segments with one end starting in a particular layer. In a chain of length l, for unit n in the range $2 \le n \le l-1$, $G^{(n)}(x_0, x|\beta_2, \beta_1)$ is proportional to the probability that a chain segment of $n+1$ units has unit 0 on layer x_0 and unit n on layer x, its last bond is of type β_1, and its second last bond is type β_2. Propagators of type Q describe chain segments ending on a particular layer, irrespective of where the other end is. Specifically, for this unit n, $Q^{(n)}(x|\beta_2, \beta_1)$ is proportional to the probability that a chain segment of $n+1$ units has unit 0 on layer x, its first bond is of type β_1 and its second bond is type β_2, but the location of the last unit is unspecified. These definitions are slightly modified for units near the chain ends.

We start with $\langle S_{\mathrm{CD}}^{(1)}(x)\rangle$, which is the average order parameter of all the units of a given chain when they visit a particular layer x. There are N_l^j these molecules of type j, and each has two chains with l_j units. Since one half of the molecules are on each side of the bilayer, N_l^j is also the number of *chains* of length l_j anchored to each side.

In an attempt to somewhat simplify the notation, we introduce $N=N_l^j$ and $l=l_j$, temporarily suppressing the subscript j. We are interested first in the N chains anchored on the left, at $x=0$. We label these N chains by i, and the configuration of chain i at a given time by γ_i. For any configuration, each carbon unit will be on some layer. (There could be more than one unit on a given layer.) We denote the layer occupied by unit n when the chain is in γ_i by $x_n^{\gamma_i}$, and the order parameter associated with it by $S_{\mathrm{CD}}^{\gamma_i}(n)$. The total number of carbon units on layer x due to all these chains is

$$N_{\mathrm{C}}(x) = \sum_{i=1}^{N} \sum_{n=1}^{l} \delta(x - x_n^{\gamma_i}) \tag{A1}$$

and the average of the order parameters of all these units is

$$\langle S_{\mathrm{CD}}^{(1)}(x)\rangle = \frac{1}{N_{\mathrm{C}}(x)} \sum_{i=1}^{N} \sum_{n=1}^{l} \delta(x - x_n^{\gamma_i}) S_{\mathrm{CD}}^{\gamma_i}(n). \tag{A2}$$

We can transform these sums over chains to sums over the configurations of a single chain by

$$\sum_{i=1}^{N} \cdots \rightarrow N \sum_{\gamma} P_\gamma \cdots, \tag{A3}$$

where P_γ is the probability that a chain is in configuration γ. We then have

$$N_{\mathrm{C}}(x) = N \sum_{\gamma} P_\gamma \sum_{n=1}^{l} \delta(x - x_n^{\gamma}) = N \sum_{\gamma} P_\gamma C_\gamma(x), \tag{A4}$$

where

$$C_\gamma(x) = \sum_{n=1}^{l} \delta(x - x_n^{\gamma}) \tag{A5}$$

is the number of carbons on layer x due to the single chain when it is in configuration γ. We can also write

$$\langle S_{\mathrm{CD}}^{(1)}(x)\rangle = \frac{1}{\sum_\gamma P_\gamma C_\gamma(x)} \sum_\gamma P_\gamma \sum_{n=1}^{l} \delta(x - x_n^\gamma) S_{\mathrm{CD}}^\gamma(n). \tag{A6}$$

These last two expressions do not involve the total number of lipids.

The next steps reexpress these in terms of the propagators. We note first that we can write $S_{\mathrm{CD}}^\gamma(n)$ as

$$S_{\mathrm{CD}}^\gamma(n) = \begin{cases} P_{\mathrm{CD}}(n, \alpha_n^\gamma, \alpha_{n+1}^\gamma), & \text{for } n = 1, \ldots, l-1, \\ P_{\mathrm{CD}}(l, \alpha_l^\gamma), & \text{for } n = l, \end{cases} \tag{A7}$$

where α_n^γ and α_{n+1}^γ are the bonds ending and beginning at carbon n, $P_{\mathrm{CD}}(n, \alpha_n^\gamma, \alpha_{n+1}^\gamma)$ is defined in Eq. (29), and

$$P_{\mathrm{CD}}(l, \alpha_l^\gamma) = \tfrac{1}{2}\{3\cos^2[\theta_{\mathrm{CD}}(l)] - 1\} \tag{A8}$$

for the last unit, with an average over the three C-D bonds.

For the numerator of Eq. (A6), we can write

$$\begin{aligned} P_\gamma \delta(x - x_n^\gamma) S_{\mathrm{CD}}^\gamma(n) &= P_\gamma \delta(x - x_n^\gamma) P_{\mathrm{CD}}(n, \alpha_n^\gamma, \alpha_{n+1}^\gamma) \\ &= \sum_{\beta_1, \beta_1'} P_\gamma \delta(x - x_n^\gamma) P_{\mathrm{CD}}(n, \beta_1, \beta_1') \\ &\quad \times \delta_{\alpha_n^\gamma, \beta_1} \delta_{\alpha_{n+1}^\gamma, \beta_1'} \end{aligned} \tag{A9}$$

for carbons $1, \ldots, l-1$, and

$$P_\gamma \delta(x - x_l^\gamma) S_{\mathrm{CD}}^\gamma(l) = \sum_{\beta_1} P_\gamma \delta(x - x_l^\gamma) P_{\mathrm{CD}}(l, \beta_1) \delta_{\alpha_l^\gamma, \beta_1} \tag{A10}$$

for the last one.

The remaining steps are to reexpress factors involving the P_γ in terms of the propagators. For example, $\Sigma_\gamma P_\gamma \delta(x - x_n^\gamma) \delta_{\alpha_n^\gamma, \beta_1} \delta_{\alpha_{n+1}^\gamma, \beta_1'}$ is proportional to the probability that unit n of a chain is on layer x, with C-C bond β_1 ending at n, and C-C bond β_1' starting there. From this it follows that, for the first atom, $n=1$,

$$\begin{aligned} \sum_\gamma P_\gamma \delta(x - x_1^\gamma) \delta_{\alpha_1^\gamma, \beta_1} \delta_{\alpha_2^\gamma, \beta_1'} \propto \sum_{\beta_2'} G^{(1)}(x_0, x|\beta_1) \\ \times \exp\{-[\epsilon_2(\beta_1, \beta_1') \\ + \epsilon_3(\beta_1, \beta_2')]\} Q^{(l-1)}(x|\beta_2', \beta_1'), \end{aligned} \tag{A11}$$

and there are similar expressions for the other units. The proportionality constant is obtained by normalizing the probability.

After some tedious algebra, we can write

$$\langle S_{\mathrm{CD}}^{(1)}(x)\rangle = \frac{\sum_{n=1}^{l} \mathcal{N}_n}{\sum_{n=1}^{l} \mathcal{D}_n}. \tag{A12}$$

The terms in the numerator are

$$\begin{aligned} \mathcal{N}_1 = \sum_{\beta_1} \sum_{\beta_1', \beta_2'} G^{(1)}(x_0, x|\beta_1) e^{-[\epsilon_2(\beta_1, \beta_1') + \epsilon_3(\beta_1, \beta_2')]} \\ \times S_{\mathrm{CD}}(\beta_1, \beta_1') Q^{(l-1)}(x|\beta_2', \beta_1'), \end{aligned} \tag{A13}$$

$$\begin{aligned} \mathcal{N}_n = \sum_{\beta_1, \beta_2} \sum_{\beta_1', \beta_2'} G^{(n)}(x_0, x|\beta_2, \beta_1) e^{-[\epsilon_2(\beta_1, \beta_1') + \epsilon_3(\beta_2, \beta_1') + \epsilon_3(\beta_1, \beta_2')]} \\ \times S_{\mathrm{CD}}(\beta_1, \beta_1') Q^{(l-n)}(x|\beta_2', \beta_1'), \end{aligned} \tag{A14}$$

for $2 \le n \le l-2$,

$$\begin{aligned} \mathcal{N}_{l-1} = \sum_{\beta_1, \beta_2} \sum_{\beta_1'} G^{(l-1)}(x_0, x|\beta_2, \beta_1) e^{-[\epsilon_2(\beta_1, \beta_1') + \epsilon_3(\beta_2, \beta_1')]} \\ \times S_{\mathrm{CD}}(\beta_1, \beta_1') Q^{(1)}(x|\beta_1') \end{aligned} \tag{A15}$$

and

$$\mathcal{N}_l = \sum_{\beta_1, \beta_2} G^{(l)}(x_0, x|\beta_2, \beta_1) S_{\mathrm{CD}}(\beta_1). \tag{A16}$$

The S_{CD} factors here are $S_{\mathrm{CD}}(\beta_1, \beta_1') = P_{\mathrm{CD}}(n, \beta_1, \beta_1')$ for all but the last carbon. For the three C-D bonds on the last carbon, $S_{\mathrm{CD}}(\beta_1) = P_{\mathrm{CD}}(l, \beta_1)$, with values $\pm 1/6$ on the diamond lattice. The expressions for the terms in the denominator, the $\mathcal{D}_n$, are the same as for the $\mathcal{N}_n$, except that the S_{CD} factors do not appear.

We also want $\langle S_{\mathrm{CD}}(x)\rangle$, the average order parameter of all the units on layer x due to all the chains, long and short, starting from either side of the bilayer. We begin by returning to the description of the bilayer with all the chains in various configurations. We need to reintroduce the label j to denote long and short chains, and the label σ for chains starting on each side, 1 or 2. We use N^{j1} and N^{j2} to denote the number of chains of length l_j starting from each side. Since there are N_l^j molecules of type j, there are $2N_l^j$ chains, and $N^{j1} = N^{j2} = N_l^j$.

Let γ_i^j denote the configuration of chain i of type j. The configuration includes the side it starts from. With this notation, the total number of carbons in layer x due to all the chains can be written

$$N_{\mathrm{C}}(x) = \sum_{j=1}^{2} \sum_{i=1}^{2N_l^j} \sum_{n=1}^{l_j} \delta(x - x_m^{\gamma_i^j}) \tag{A17}$$

and $\langle S_{\mathrm{CD}}(x)\rangle$ can be written

$$\langle S_{\mathrm{CD}}(x)\rangle = \frac{1}{N_{\mathrm{C}}(x)} \sum_{j=1}^{2} \sum_{i=1}^{2N_l^j} \sum_{n=1}^{l_j} \delta(x - x_m^{\gamma_i^j}) S_{\mathrm{CD}}^{\gamma_i^j}(n). \tag{A18}$$

Proceeding as above, we transform from sums over all the chains to sums over configurations of typical chains, via

$$\sum_{i=1}^{2N_l^j} \cdots \to \sum_{\sigma=1}^{2} \sum_{\gamma^{j\sigma}} N^{j\sigma} P_{\gamma^{j\sigma}} \cdots, \tag{A19}$$

where $\gamma^{j\sigma}$ labels each possible configuration of a chain of length j, starting from side σ, and $P_{\gamma^{j\sigma}}$ is the probability that a chain of this length is in this configuration and starts at that side.

A key point is that all the summations in Eq. (A17) and (A18) separate into sums over short and long chains, and chains starting from each side. The end result is that we can write $\langle S_{\mathrm{CD}}(x)\rangle$ as

$$\langle S_{\mathrm{CD}}(x)\rangle = \frac{1}{\langle\rho(x)\rangle}\sum_{j=1}^{2}\left[\langle\rho^{j1}(x)\rangle\langle S_{\mathrm{CD}}^{j1,(1)}(x)\rangle + \langle\rho^{j2}(x)\rangle\langle S_{\mathrm{CD}}^{j2,(1)}(x)\rangle\right]. \tag{A20}$$

In this expression, $\langle\rho^{j1}(x)\rangle$ and $\langle\rho^{j2}(x)\rangle$ are the density of carbons on layer x due to chains of length j that start on side $\sigma=1$ and 2, respectively, and $\langle\rho(x)\rangle$ is the total density on layer x,

$$\langle\rho(x)\rangle = \sum_{j=1}^{2}\sum_{\sigma=1}^{2}\langle\rho^{j\sigma}(x)\rangle. \tag{A21}$$

Each $\langle S_{\mathrm{CD}}^{j1,(1)}(x)\rangle$ is the same as $\langle S_{\mathrm{CD}}^{(1)}(x)\rangle$ defined in Eqs. (A2) and (A12): The order parameter at layer x due to chains of type j starting from side $\sigma=1$. $\langle S_{\mathrm{CD}}^{j2,(1)}(x)\rangle$ is the same thing, but for chains starting from the other side. Thus, we can interpret Eq. (A20) as a weighted average of the order parameters of all the units on a layer x at a given time.

The properties of chains starting from each side satisfy simple symmetry properties, namely

$$\langle\rho^{j2}(x)\rangle = \langle\rho^{j1}(t_C - x)\rangle \tag{A22}$$

and

$$\langle S_{\mathrm{CD}}^{j,(2)}(x)\rangle = \langle S_{\mathrm{CD}}^{j,(1)}(t_C - x)\rangle, \tag{A23}$$

which simplify the actual calculations in Eqs. (A20) and (A21).

APPENDIX B: SEGMENT DISTRIBUTIONS

We define the segment distribution function, $P_j(n,x)$, as the probability that carbon n is on layer x. We calculate it here for a particular chain length j, for chains starting from side 1 at $x=0$. Of course, the distribution functions for chains from the other side are simply related by symmetry. Again, we temporarily suppress the label j to ease the notation.

The $P(n,x)$ have certain simple properties that are easy to specify. All units are constrained to the bilayer interior, so $P(n,x)=0$ at $x=0$ and $x=t_C$. Second, the farthest that carbon n can penetrate into the layer is to $x=n$, and that is only if the first n bonds are fully ordered. Thus we have the additional result that $P(n,x)=0$ for $x>n$ for each n.

We again use the propagators. Consider, first, any carbon n between numbers 2 and $l-2$. The probability that this carbon is on layer x is proportional to

$$P(n,x) \propto \sum_{\beta_1,\beta_2}\sum_{\beta_1',\beta_2'} G^{(n)}(x_0,x|\beta_2,\beta_1) \times e^{-[\epsilon_2(\beta_1,\beta_1')+\epsilon_3(\beta_2,\beta_1')+\epsilon_3(\beta_1,\beta_2')]}Q^{(l-n)}(x|\beta_2',\beta_1'). \tag{B1}$$

The normalization constant can be calculated by the requirement that each carbon must be somewhere, i.e.,

$$\sum_x P(n,x) = 1. \tag{B2}$$

Summing the right-hand side of Eq. (B1) over all layers is equal to $\Sigma_{\beta_1',\beta_2'}Q^{(l)}(x_0|\beta_2',\beta_1')$, which is also proportional to the sum of the probabilities of all the configurations. From this it follows that the normalized distribution functions for units in the range $2\le n\le l-2$ are

$$P(n,x) = \frac{1}{\mathcal{D}_S}\sum_{\beta_1,\beta_2}\sum_{\beta_1',\beta_2'} G^{(n)}(x_0,x|\beta_2,\beta_1) \times e^{-[\epsilon_2(\beta_1,\beta_1')+\epsilon_3(\beta_2,\beta_1')+\epsilon_3(\beta_1,\beta_2')]}Q^{(l-n)}(x|\beta_2',\beta_1') \tag{B3}$$

with

$$\mathcal{D}_S = \sum_{\beta_1',\beta_2'} Q^{(l)}(x_0|\beta_2',\beta_1'). \tag{B4}$$

For the other units, they are given by

$$P(1,x) = \frac{1}{\mathcal{D}_S}\sum_{\beta_1}\sum_{\beta_1',\beta_2'} G^{(1)}(x_0,x|\beta_1) \times e^{-[\epsilon_2(\beta_1,\beta_1')+\epsilon_3(\beta_1,\beta_2')]}Q^{(l-1)}(x|\beta_2',\beta_1'), \tag{B5}$$

$$P(l-1,x) = \frac{1}{\mathcal{D}_S}\sum_{\beta_1,\beta_2}\sum_{\beta_1'} G^{(l-1)}(x_0,x|\beta_2,\beta_1) \times e^{-[\epsilon_2(\beta_1,\beta_1')+\epsilon_3(\beta_2,\beta_1')]}Q^{(1)}(x|\beta_1'), \tag{B6}$$

and

$$P(1,x) = \frac{1}{\mathcal{D}_S}\sum_{\beta_1,\beta_2} G^{(1)}(x_0,x|\beta_2,\beta_1). \tag{B7}$$

Although the index j has been suppressed in these expressions, the reader is reminded that these quantities depend on the chain length, so the appropriate l_j must be used throughout.

[1] G. Cevc and D. Marsh, *Phospholipid Bilayers: Physical Principles and Models* (Wiley-Interscience, New York, 1987).

[2] Dalian Lu, D. Singh, M. R. Morrow, and C. W. M. Grant, Biochemistry **32**, 290 (1993).

[3] A. Seelig and J. Seelig, Biochemistry **13**, 4839 (1974).

[4] D. Marsh, A. Watts, and I. C. P. Smith, Biochemistry **22**, 3023 (1983).

[5] R. L. Thurmond, S. W. Dodd, and M. F. Brown, Biophys. J.

59, 108 (1991).
[6] M. R. Morrow and Dalian Lu, Chem. Phys. Lett. **182**, 435 (1991).
[7] M. R. Morrow, J. P. Whitehead, and D. Lu, Biophys. J. **63**, 18 (1992).
[8] Dalian Lu, I. Vavasour, and M. R. Morrow, Biophys. J. **68**, 574 (1995).
[9] M. D. Whitmore, J. P. Whitehead, and A. Roberge, Can. J. Phys. **76**, 831 (1998).
[10] M. D. Whitmore and J. P. Whitehead, Can. J. Phys. **76**, 883 (1998).
[11] F. A. M. Leermakers and J. M. H. M. Scheutjens, J. Chem. Phys. **89**, 3264 (1988).
[12] F. A. M. Leermakers and J. M. H. M. Scheutjens, J. Chem. Phys. **89**, 6912 (1988).
[13] L. A. Meijer, F. A. M. Leermakers, and J. Lyklema, Recl. Trav. Chim. Pays-Bas **113**, 167 (1994).
[14] L. A. Meijer, F. A. M. Leermakers, and J. Lyklema, J. Phys. Chem. **99**, 17282 (1995).
[15] E. A. DiMarzio, J. Chem. Phys. **66**, 1160 (1976).
[16] J. F. Nagle and D. A. Wilkinson, Biophys. J. **23**, 159 (1978).
[17] J. R. Trudell, D. G. Payan, J. H. Chin, and E. N. Cohen, Biochim. Biophys. Acta **373**, 436 (1974).
[18] N.-I. Liu and R. L. Kaye, Biochemistry **16**, 3484 (1977).
[19] J. Stamatoff, D. Guillon, L. Powers, and P. Cladis, Biochem. Biophys. Res. Commun. **85**, 724 (1978).
[20] F. Ceuterick, J. Peeters, K. Heremans, H. De Smedt, and H. Olbrechts, Eur. J. Biochem. **87**, 401 (1978).
[21] D. B. Mountcastle, R. L. Biltonen, and M. J. Halsey, Proc. Natl. Acad. Sci. U.S.A. **75**, 4906 (1978).
[22] P. L.-G. Chong and G. Weber, Biochemistry **22**, 5544 (1983).
[23] P. T. T. Wong and H. H. Mantsch, Biochemistry **24**, 4091 (1985).
[24] S. Utoh and T. Takemura, Jpn. J. Appl. Phys., Part 1 **24**, 356 (1985).
[25] R. E. Tosh and P. J. Collings, Biochim. Biophys. Acta **859**, 10 (1986).
[26] L. F. Braganza and D. L. Worcester, Biochemistry **25**, 2591 (1986).
[27] S. K. Prasad, R. Shashidhar, B. P. Gaber, and S. C. Chandrasekhar, Chem. Phys. Lipids **43**, 227 (1987).
[28] P. T. T. Wong, D. J. Siminovitch, and H. H. Mantsch, Biochim. Biophys. Acta **947**, 139 (1988).
[29] R. Winter and W.-C. Pilgrim, Ber. Bunsenges. Phys. Chem. **93**, 708 (1989).
[30] D. A. Driscoll, J. Jonas, and A. Jonas, Chem. Phys. Lipids **58**, 97 (1991).
[31] S. Haneshina, K. Tamura, H. Kawakami, and H. Matsuki, Chem. Lett. **1992**, 1963 (1992).
[32] B. B. Bonev and M. R. Morrow, Phys. Rev. E **55**, 5825 (1997).